



## ORIGINAL ARTICLE

# Novel visible-light-driven photocatalyst of NiO/Cd/g-C<sub>3</sub>N<sub>4</sub> for enhanced degradation of methylene blue

Mohammad Ali Karimi<sup>a,\*</sup>, Mojdeh Atashkadi<sup>a</sup>, Mehdi Ranjbar<sup>b</sup>,  
Aziz Habibi-Yangjeh<sup>c</sup>

<sup>a</sup> Department of Chemistry, Payame Noor University, 19395-4697 Tehran, Iran

<sup>b</sup> Pharmaceutics Research Center, Institute of Neuropharmacology, Kerman University of Medical Sciences, Kerman, Iran

<sup>c</sup> Department of Chemistry, Faculty of Sciences, University of Mohaghegh Ardabili, Ardabil, Iran

Received 8 February 2020; accepted 14 April 2020

Available online 23 April 2020

## KEYWORDS

NiO/Cd/g-C<sub>3</sub>N<sub>4</sub> ternary  
nanocomposites;  
Microwave-assisted synthe-  
sis;  
Methylene blue;  
UV/Vis spectroscopy

**Abstract** Novel NiO/Cd/g-C<sub>3</sub>N<sub>4</sub> photocatalysts were synthesized using a green and straightforward microwave-assisted method and characterized by X-ray diffraction (XRD), Fourier-transform infrared spectroscopy (FT-IR), the Brunauer–Emmett–Teller (BET) method, transmission electron microscopy (TEM), scanning electron microscopy (SEM), energy-dispersive X-ray spectroscopy (EDS), and ultraviolet–visible spectroscopy (UV–Vis). The ternary NiO/Cd/g-C<sub>3</sub>N<sub>4</sub> nanocomposites were evaluated for the degradation of methylene blue (MB) at room temperature under the visible light irradiation. Experimental results revealed that the weight percent of cadmium had a remarkable effect on the photodegradation efficiency. The NiO/Cd/g-C<sub>3</sub>N<sub>4</sub> (0.1%) sample exhibited superior activity in the degradation reaction. The activity of this nanocomposite was about 4.5 and 3.25 fold higher than those of the pure g-C<sub>3</sub>N<sub>4</sub> and NiO/g-C<sub>3</sub>N<sub>4</sub> samples in the degradation of MB, respectively. The enhanced photocatalytic activity was attributed to the low energy gap, increased absorption capacity of the visible light, and efficient suppression of the recombination of photogenerated electron-hole pairs. A detailed photocatalytic mechanism over the nanocomposite of NiO/Cd/g-C<sub>3</sub>N<sub>4</sub> (0.1%) was proposed with superoxide radical anion  $\cdot\text{O}_2^-$  as the main reactive species. The stability of the nanocomposite was confirmed after four consecutive runs as well.

© 2020 Published by Elsevier B.V. on behalf of King Saud University. This is an open access article under the CC BY-NC-ND license (<http://creativecommons.org/licenses/by-nc-nd/4.0/>).

## 1. Introduction

Among various kinds of environmental purifying treatments, nanocomposite-based photocatalysis is a green, biocompatible, and low-cost technology that successfully eliminates the threats to human health and ecological security (Nezar et al., 2018; Jeejamol et al., 2018; Mella et al., 2017). Today many studies are done to find visible-light-driven photocatalysts for degra-

\* Corresponding author.

E-mail address: [m\\_karimi@pnu.ac.ir](mailto:m_karimi@pnu.ac.ir) (M.A. Karimi).

Peer review under responsibility of King Saud University.



dation of organic pollutants (Babu et al., 2019). Graphitic carbon nitride (g-C<sub>3</sub>N<sub>4</sub>) has captured much attention in this regard (Allahresani et al., 2017). It is a polymeric semiconductor that has been widely used in the decomposition of organic contaminants (Nayak and Parida, 2019), hydrogen production (Patnaik et al., 2018), CO<sub>2</sub> photo-reduction (Wang et al., 2015), and water splitting (Mousavi et al., 2018). Metal-free g-C<sub>3</sub>N<sub>4</sub> is a pale yellow powder, composed of carbon and nitrogen with a theoretical ratio of 0.75 (Yin et al., 2015). It is easily synthesized by abundant nitrogen-rich precursors such as urea, thiourea, melamine, cyanamide, and dicyandiamide (Martha et al., 2013; Wu et al., 2018). It enjoys excellent properties such as thermal and chemical stability (Das et al., 2020), extreme hardness (Mousavi and Habibi-Yangjeh, 2018), non-toxicity (Yan et al., 2009), biocompatibility (Su et al., 2016), unique 2D structure (Xu et al., 2015), and narrow bandgap of 2.7 eV (Akhundi and Habibi-Yangjeh, 2017). However, due to the rapid recombination of photoinduced electron-hole pairs (Patnaik et al., 2018), low visible-light absorption capacity (Cui et al., 2016), and insufficient surface active sites (Lu et al., 2019), the pure g-C<sub>3</sub>N<sub>4</sub> suffers from the slow reaction kinetics in photocatalysis (Bian et al., 2012; Zhou et al., 2018). So different measures for modification of g-C<sub>3</sub>N<sub>4</sub> are proposed to overcome the above drawbacks. One of these is coupling g-C<sub>3</sub>N<sub>4</sub> with semiconductors, metal oxides, metal sulfides, metal-free components, noble metals, halides, and composite oxides that have proper energy levels in their bandgap (Akhundi and Habibi-Yangjeh, 2015; Lai et al., 2018; Allahresani et al., 2018). Dopants have direct effects on increasing visible-light harvesting ability, enlarging the specific surface area, and suppressing the recombination of photogenerated electron-hole pairs (Deng et al., 2018; Babu et al., 2018). They maximize the lifetime of charge carriers and improve the stability and activity of g-C<sub>3</sub>N<sub>4</sub>-based photocatalysts (Lu et al., 2017; Nayak and Parida, 2018). The correlation between the amount of light absorption and/or surface area with the photocatalytic efficiency is proportional, the larger amount of light absorption and/or more active surface area, the higher photocatalytic efficiency is expected (Wen et al., 2017). In recent years, many investigations have been carried out about combining g-C<sub>3</sub>N<sub>4</sub> with different dopants like NiO and Cd compounds. Wang et al. prepared g-C<sub>3</sub>N<sub>4</sub>/NiO p-n heterojunction materials with ball-flower morphology and showed the enhanced photocatalytic performance for the removal of tetracycline and Cr<sup>6+</sup> pollutants (Wang et al., 2019). Zhang et al. reported ultrasound exfoliation of g-C<sub>3</sub>N<sub>4</sub> with the assistance of cadmium ions with efficient photocatalytic activity for the degradation of methyl orange (Zhang et al., 2016). Moreover, Lu et al. synthesized atomic layer g-C<sub>3</sub>N<sub>4</sub>/CdS heterojunctions with the enhanced visible-light photocatalytic activity (Lu et al., 2014).

Herein, we report the fabrication of visible-light-driven photocatalyst by introducing of nickel oxide and cadmium into the pristine g-C<sub>3</sub>N<sub>4</sub> to prepare the ternary NiO/Cd/g-C<sub>3</sub>N<sub>4</sub> photocatalyst. Due to synergistic effects, found within the heterogeneous structures of the ternary photocatalysts, remarkable enhancement in the photoactivity is observed (Wen et al., 2017; Zhou et al., 2017). To the best of our knowledge, this is the first study to describe the ternary NiO/Cd/g-C<sub>3</sub>N<sub>4</sub> co-catalysts. We benefited a lot from the microwave absorption properties of g-C<sub>3</sub>N<sub>4</sub> (Green et al., 2018) and followed the facile, low temperature, short time, and energy-

saving microwave-assisted synthesis method. The structure, morphology and physicochemical properties of the samples were characterized by XRD, FT-IR, BET, TEM, SEM, EDS, and UV-Vis analytical techniques. As expected, doping with a metal oxide (NiO) and a metal element (Cd) enhanced the visible-light responsive photocatalytic activity of the g-C<sub>3</sub>N<sub>4</sub> through making the desired band structure and promoting electron transfer rate. In the present work, the influence of weight percent of cadmium on the photodegradation efficiency was also investigated, and a possible mechanism for the superior photocatalytic performance was proposed. Finally, the stability of the NiO/Cd/g-C<sub>3</sub>N<sub>4</sub> photocatalyst was tested for four successive runs.

## 2. Experimental

### 2.1. Materials

Melamine, nickel(II) nitrate hexahydrate, sodium hydroxide, ethanol, glucose, methylene blue hydrate, cadmium acetate dehydrate were employed without further purification. Deionized (DI) water was used in all of the experiments.

### 2.2. Instruments

The XRD analysis patterns were obtained on PHILIPS X'PERT PRO X-ray diffractometer using Cu-K $\alpha$  radiation ( $\lambda = 1.5406 \text{ \AA}$ ,  $2\theta = 10\text{--}80^\circ$ ) to study the crystalline structure of the samples. The FT-IR chemical analysis spectra were recorded on SHIMADZU IRPRESTIGE-21 IR spectrophotometer using KBr method in the range of 400–4000 cm<sup>-1</sup>. The N<sub>2</sub> adsorption-desorption isotherms were measured by BELSORP MINI II apparatus at 196 °C. Before the analysis, the BEL PREP VAC II degassed the samples at 120 °C for 15 h. The data of specific surface areas were calculated with the Brunauer-Emmett-Teller (BET) method. The TEM structural morphologies were investigated by PHILIPS CM 120 apparatus. The SEM surface morphologies and EDS elemental mapping micrographs were collected by MIRA III VEGA-TESCAN-XMU instrument. Before the analysis, samples were mounted on aluminum stubs using double-sided adhesive tapes and coated with a thin layer of gold. The UV-Vis spectra were achieved on GBC CINTRA 20 apparatus in the wavelength range of 200–800 nm.

### 2.3. Preparation of photocatalysts

Melamine (5 g) as the precursor of g-C<sub>3</sub>N<sub>4</sub> was put in a covered alumina crucible and calcined at 550 °C for four hours; then, it cooled down to room temperature. The pale yellow g-C<sub>3</sub>N<sub>4</sub> solid was ground into the light powder and collected for further use. Afterward, nickel nitrate (0.22 g) as the precursor and sodium hydroxide (0.44 g) as the precipitating agent were dissolved in DI water (100 ml) and heated at 60 °C for 45 min to form NiO solution. Then cadmium acetate (300 mg) as the precursor of cadmium (0.05, 0.1, 0.2, 0.4, and 0.5 wt%) was obtained. When air annealing, acetate totally or partially decomposed and produced volatile compounds and traces of carbon, so no impure substance influenced the photocatalytic efficiency.

For fabrication of the NiO/Cd/g-C<sub>3</sub>N<sub>4</sub> photocatalyst, g-C<sub>3</sub>N<sub>4</sub> (300 mg) and glucose (90 mmol) as the natural nanoparticles stabilizer were dispersed in ethanol/DI water 1:1 (10 ml) and heated at 60 °C for 30 min using a magnetic stirrer. Then NiO solution and cadmium acetate were slowly added to the mixture. The obtained suspension was refluxed at 60 °C for 60 min, treated with ultrasound for 45 min and refluxed again at 60 °C for three hours (Ostwald ripening precipitation). After adjusting pH to eight and centrifugal separation, the precipitate was put in a microwave. It was exposed to MW radiation (600 W) for 5 min as 2 min on and 1 min off and finally cooled at room temperature. Then, the NiO/Cd/g-C<sub>3</sub>N<sub>4</sub> precipitate was rinsed with ethanol and DI water several times and dried at 60 °C for 24 h. The as-prepared photocatalysts were labeled as NiO/Cd/g-C<sub>3</sub>N<sub>4</sub> (X%), where X represents the weight percent of cadmium. Meanwhile, the NiO/g-C<sub>3</sub>N<sub>4</sub> sample was synthesized under the same conditions. The whole mechanism of the experimental synthesis is documented in [Scheme 1](#).

#### 2.4. Photocatalysis experiments

The photocatalytic activity of the as-synthesized nanocomposites was evaluated by the degradation of MB as a model cationic dye under the visible light irradiation. The experiments were done inside the enclosed wooden reactor system. It was

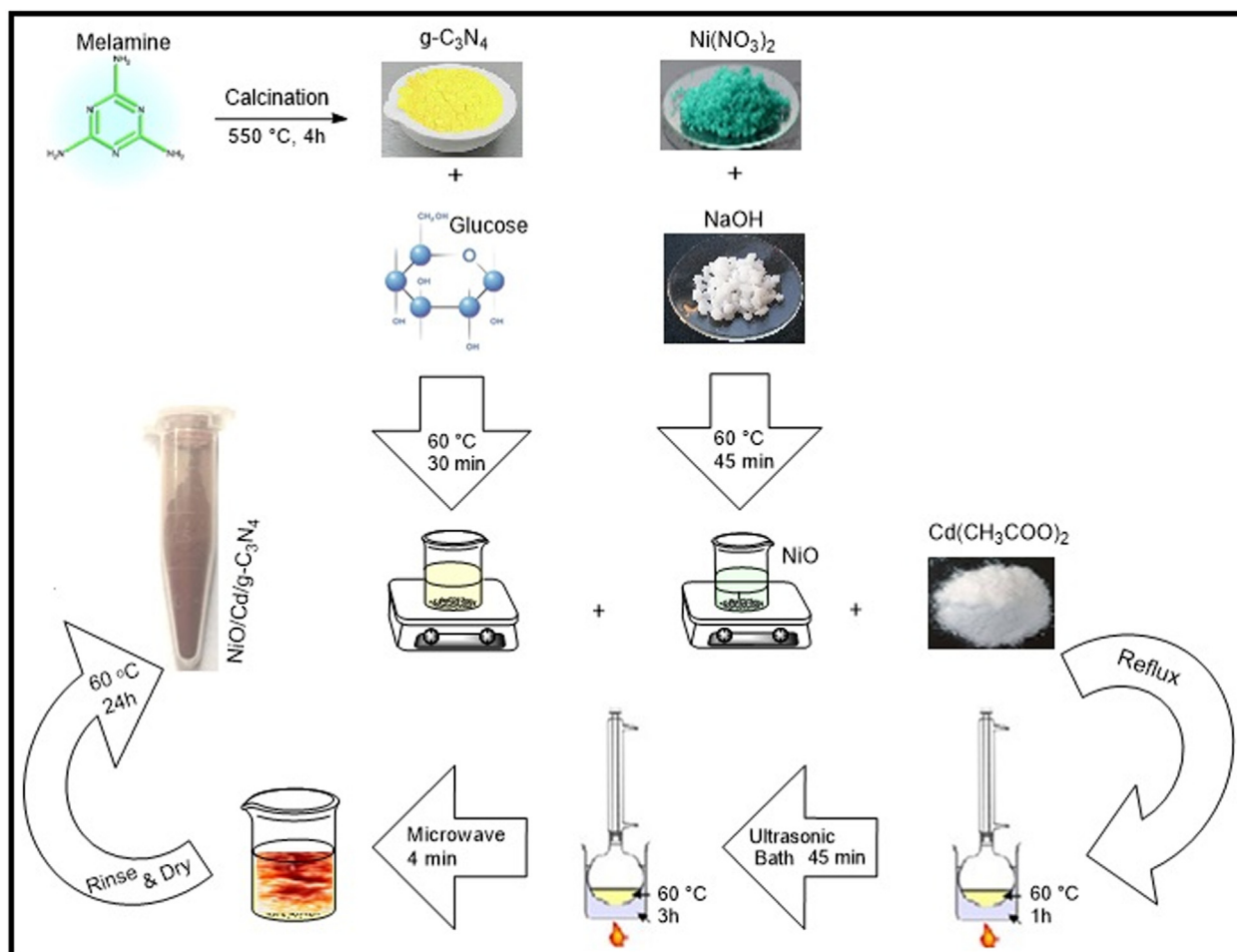
equipped with a 50 W LED lamp to supply the visible illumination, a small air ventilator to supply oxygen, a water jacket to keep the temperature of the system at room temperature, and a Pyrex glassware reactor to contain MB aqueous solution. Before illumination, the nanocomposite (0.1 g) was dispersed into an MB solution (100 ml,  $3 \times 10^{-5}$  M). The suspension was mechanically stirred for 30 min to reach the adsorption–desorption equilibrium in the dark. The first sample (2 ml) was afterward taken and called “sample at zero times of illumination”; then, the reaction solution was placed under the visible light irradiation, and samples were taken every 10 min for 90 min. The samples were finally centrifuged at 4000 rpm for 4 min to get the precipitate out. The absorbance of the samples was measured at 664 nm ( $\lambda_{\text{max}}$  of MB) with a UV–Vis spectrophotometer. The photodegradation rate ( $\eta$ ) of MB was calculated as follows:

$$\eta = (A_0 - A_t)/A_0 \times 100\% \quad (1)$$

where  $A_0$  is the initial absorbance of MB and  $A_t$  is the absorbance at the time ( $t$ ) ([Han et al., 2018](#)).

#### 2.5. Reactive species trapping experiments

The radical trapping experiments determined the active species during the photocatalytic reaction. The  $\cdot\text{O}_2^-$  and  $\cdot\text{OH}$  radicals



**Scheme 1** The schematic diagram for the preparation of the NiO/Cd/g-C<sub>3</sub>N<sub>4</sub> nanocomposites.

plus the holes were scavenged by benzoquinone (BQ), isopropanol (2-PrOH) and potassium iodide (KI), respectively.

### 3. Results and discussion

#### 3.1. Photocatalysts characterization

The XRD patterns of the g-C<sub>3</sub>N<sub>4</sub>, NiO/g-C<sub>3</sub>N<sub>4</sub>, and NiO/Cd/g-C<sub>3</sub>N<sub>4</sub> (0.1%) nanocomposites are shown in Fig. 1. Typically, two distinct diffraction peaks at 13.1° and 27.4° correspond to the (1 0 0) and (0 0 2) lattice planes of the g-C<sub>3</sub>N<sub>4</sub>, respectively (JCPDS 87-1526). The diffraction of the (1 0 0) plane matches the tri-s-triazine unit structure, the precursor of melamine. The ring structure of the tri-s-triazine reduces the bond reaction barrier between carbon and nitrogen to enhance the crystalline characteristic of the graphitic nanostructure layers. The diffraction of the (0 0 2) plane corresponds to the interlayer accumulation of conjugated aromatic compounds, representing the graphitic structure. The XRD patterns of the NiO/g-C<sub>3</sub>N<sub>4</sub> and NiO/Cd/g-C<sub>3</sub>N<sub>4</sub> (0.1%) samples exhibit similar peak positions to that of the g-C<sub>3</sub>N<sub>4</sub>. They confirm that doping with NiO and Cd species do not change the lattice structure of g-C<sub>3</sub>N<sub>4</sub>, but reduce the crystallinity by decreasing diffraction intensity. The characteristic peaks of NiO and Cd particles are observed. Compared with the XRD pattern of the NiO/g-C<sub>3</sub>N<sub>4</sub>, a shift is seen on the two peaks at about 55° and 67° in that of the NiO/Cd/g-C<sub>3</sub>N<sub>4</sub> sample. It might be due to various factors such as crystallite size, orientation, shape, stress, and thermal annealing. The absence of additional peaks confirms the formation of the photocatalyst without any impurity.

The FT-IR spectra of the g-C<sub>3</sub>N<sub>4</sub>, NiO/g-C<sub>3</sub>N<sub>4</sub>, and NiO/Cd/g-C<sub>3</sub>N<sub>4</sub> (0.1%) nanocomposites are presented in Fig. 2. The broad absorption bands around 3400 cm<sup>-1</sup> are corresponding to the O—H stretching vibration of water molecules adsorbed on the surface of nanocomposites (Karimi et al.,

2015). The absorption peaks at about 2900 cm<sup>-1</sup> are assigned to the stretching vibration of the C—H bond (Li et al., 2015). The C—N heterocycles stretching vibrations are observed at around 1600 cm<sup>-1</sup> (Li et al., 2018), and the C—O stretching vibrations are located at 1050 cm<sup>-1</sup> (Habibi and Rahmati, 2014). Two weak and broad peaks around 684 and 1394 cm<sup>-1</sup> are ascribed to the presence of Cd (Peng et al., 2016). The absorption peak at 570 cm<sup>-1</sup> originates from the stretching vibration of the Ni—O bond (Dharmaraj et al., 2006). The results confirm that NiO and Cd particles successfully interact with the pure g-C<sub>3</sub>N<sub>4</sub> to form binary and ternary nanocomposites.

The N<sub>2</sub> adsorption–desorption isotherms analyses of the samples are shown in Fig. 3. The specific surface areas calculated by the BET method are 15, 35 and 27 m<sup>2</sup> g<sup>-1</sup> for the g-C<sub>3</sub>N<sub>4</sub>, NiO/g-C<sub>3</sub>N<sub>4</sub>, and NiO/Cd/g-C<sub>3</sub>N<sub>4</sub> (0.1%) nanocomposites, respectively. The increase in the specific surface area of the NiO/g-C<sub>3</sub>N<sub>4</sub> sample might be due to the hierarchical structure formed by NiO on the g-C<sub>3</sub>N<sub>4</sub>, similar to many studies about the synthesis of the pure g-C<sub>3</sub>N<sub>4</sub> (Kumaresan et al., 2020). However, by the decoration of Cd particles on the nanocomposite of NiO/g-C<sub>3</sub>N<sub>4</sub>, the specific surface area decreases to some extent. This decrease might be related to filling or blocking some of the active sites at the surface of the NiO/g-C<sub>3</sub>N<sub>4</sub> by Cd species. These data verify that the specific surface area (SSA) of ternary nanocomposite photocatalysts do not play a major role in the enhancement of the photocatalytic activity (Nagajyothi et al., 2017).

The surface morphologies and microstructures of the g-C<sub>3</sub>N<sub>4</sub>, NiO/g-C<sub>3</sub>N<sub>4</sub>, and NiO/Cd/g-C<sub>3</sub>N<sub>4</sub> (0.1%) nanocomposites are presented in Fig. 4. SEM images (Fig. 4a–d) show the porous surface of the nanocomposites that act as adsorbents for dye molecules. As can be seen in TEM images (Fig. 4e

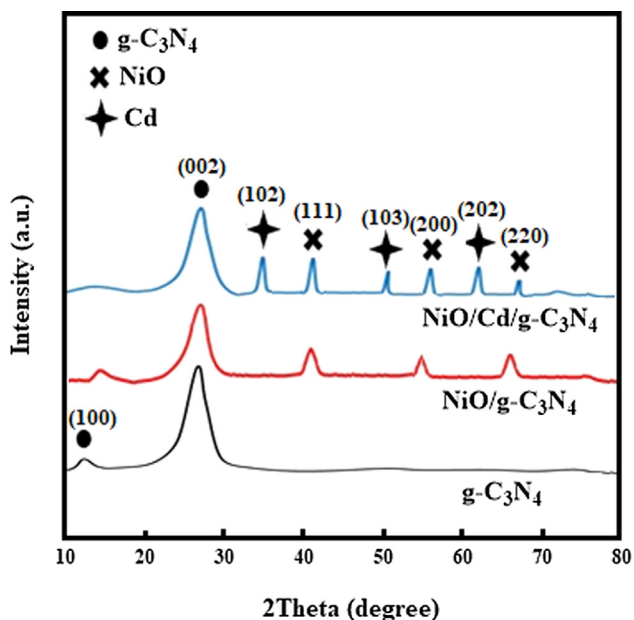


**Fig. 1** The XRD patterns of the g-C<sub>3</sub>N<sub>4</sub>, NiO/g-C<sub>3</sub>N<sub>4</sub>, and NiO/Cd/g-C<sub>3</sub>N<sub>4</sub> (0.1%) nanocomposites.

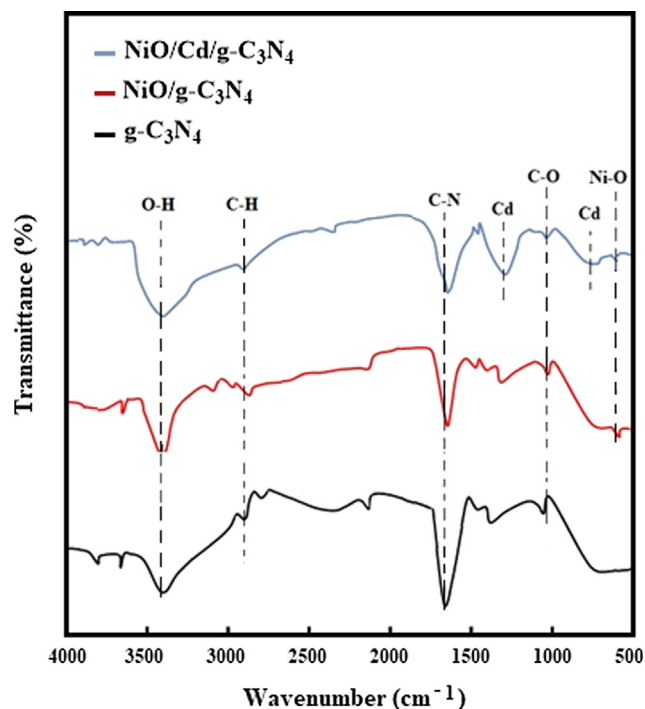


**Fig. 2** The FT-IR spectra of the g-C<sub>3</sub>N<sub>4</sub>, NiO/g-C<sub>3</sub>N<sub>4</sub>, and NiO/Cd/g-C<sub>3</sub>N<sub>4</sub> (0.1%) nanocomposites.

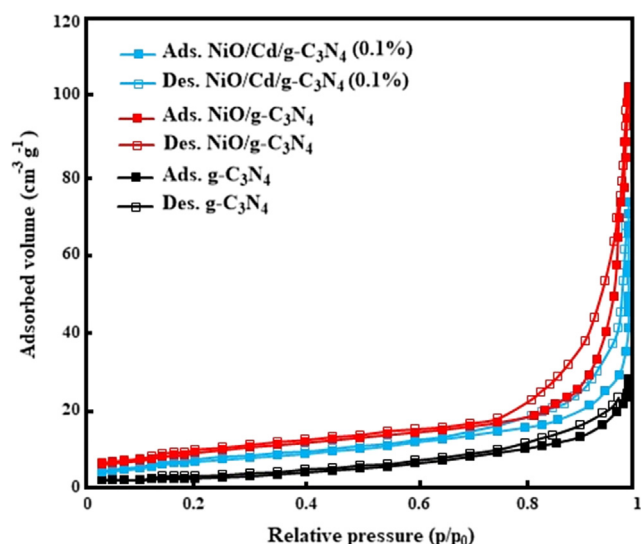


**Fig. 3** The nitrogen adsorption–desorption data for the  $g\text{-C}_3\text{N}_4$ ,  $\text{NiO}/g\text{-C}_3\text{N}_4$ , and  $\text{NiO}/\text{Cd}/g\text{-C}_3\text{N}_4$  (0.1%) nanocomposites.

and f), the nanosheets of  $g\text{-C}_3\text{N}_4$  are thin and transparent to the electron beam. The observations confirm the successful decoration of NiO and Cd species over the surface of the  $g\text{-C}_3\text{N}_4$ .

The identification and elemental mapping of the  $\text{NiO}/g\text{-C}_3\text{N}_4$  and  $\text{NiO}/\text{Cd}/g\text{-C}_3\text{N}_4$  (0.1%) nanocomposites confirmed by the EDS spectra are shown in Fig. 5. The peaks are ascribed to C, N, O, Ni, and Cd elements and detected at their proper level of energy. The results are in good harmony with other investigations and confirm the deposition of NiO and Cd species on the  $g\text{-C}_3\text{N}_4$ .

Methylene blue was selected as a common organic pollutant to evaluate the photocatalytic performance of the as-fabricated samples under visible light irradiation. Fig. 6 shows plots of the absorbance versus wavelength at different irradiation times for photodegradation of MB over binary  $\text{NiO}/g\text{-C}_3\text{N}_4$  and ternary  $\text{NiO}/\text{Cd}/g\text{-C}_3\text{N}_4$  (0.1%) nanocomposites. It is clear that the intensity of the absorption peaks at 664 nm gradually decreases without any changes in the positions. The highest photocatalytic activity is considered for ternary  $\text{NiO}/\text{Cd}/g\text{-C}_3\text{N}_4$  (0.1%) nanocomposite; MB degradation efficiency accomplishes 81.8% within 90 min photocatalytic reaction.

### 3.2. Photocatalytic activity

Plots of the absorbance of MB versus different irradiation times over the as-synthesized nanocomposites, as shown in Fig. 7a, reveal the photocatalytic activity of each sample. The behavior of the photocatalysts in the dark was also displayed to show the influence of the surface adsorption on the photocatalytic activity. As can be seen, after 30 min stirring in the light off and 90 min in the light on, the  $g\text{-C}_3\text{N}_4$  exhibited a weak performance; just 18.2% of MB molecules were photodegraded. The low photocatalytic efficiency was attributed to the rapid recombination of photogenerated electron-hole pairs and the participation of a small fraction of charge carriers in the photocatalytic reactions (Huang et al., 2017). Due to the effect of metal oxide doping on promoting separation and

migration of electrons, the nanocomposite of  $\text{NiO}/g\text{-C}_3\text{N}_4$  showed a better photocatalytic activity; 25.2% of dye molecules were degraded. Active sites on the p-type NiO, governed by the polarity of MB cationic dye, prevented linking the dye chromophores to the surface of the catalyst, resulting in low degradation efficiency (Kumar et al., 2017). The photocatalytic performance of ternary  $\text{NiO}/\text{Cd}/g\text{-C}_3\text{N}_4$  nanocomposites considerably depended on cadmium weight percent. Cd ions modified the nanocomposites to show improved photocatalytic efficiency. The photocatalytic activity of the nanocomposite of  $\text{NiO}/\text{Cd}/g\text{-C}_3\text{N}_4$  (0.05%) proceeded slowly and reached 28.2%. It revealed that Cd weight percent was not enough to eliminate the repulsive forces that existed between Ni on the surface of the photocatalyst and MB dye molecules. The optimum photocatalytic activity found to be for the  $\text{NiO}/\text{Cd}/g\text{-C}_3\text{N}_4$  (0.1%) nanocomposite. MB degradation efficiency as 81.8% was about 4.5 and 3.25 fold higher than those of the pure  $g\text{-C}_3\text{N}_4$  and  $\text{NiO}/g\text{-C}_3\text{N}_4$  samples, respectively. It was mainly ascribed to the Cd sufficient weight percent. Cd species acted as trapping sites of charge carriers, suppressed the electron-hole recombination rate, and caused more adsorption of dye molecules on the surface of the photocatalyst. However, by increasing Cd weight percent, the photocatalytic activity descended. Nearly 60, 55, and 52% of MB molecules were photodegraded over the  $\text{NiO}/\text{Cd}/g\text{-C}_3\text{N}_4$  (0.2%),  $\text{NiO}/\text{Cd}/g\text{-C}_3\text{N}_4$  (0.4%), and  $\text{NiO}/\text{Cd}/g\text{-C}_3\text{N}_4$  (0.5%) nanocomposites, respectively. It followed that cadmium-rich active sites on the surface of the nanocomposites were not chemically beneficial to absorb more visible light and degrade dye molecules. As seen, the lower photocatalytic activity was ascribed to the sample with the highest cadmium content (0.5%) (Wang et al., 2015).

Concerning the Langmuir–Hinshelwood kinetic model, photocatalytic Degradation of MB over the photocatalysts was expressed by pseudo-first-order equation at low concentrations:

$$\ln[\text{MB}] = \ln[\text{MB}]_0 - k_{\text{obs}}t \quad (2)$$

In which  $[\text{MB}]$  and  $[\text{MB}]_0$  are concentrations of MB at time of  $t$ , and zero, respectively and  $k_{\text{obs}}t$  ( $\text{min}^{-1}$ ) is the pseudo-first-order kinetic constant estimated from the slope of the linear relationship of  $\ln(C_0/C_t)$  versus  $t$  (Pirhashemi and Habibi-Yangjeh, 2013). The results of  $k_{\text{obs}}t$  calculation are shown in Fig. 7b. It appears that the weight percent of Cd greatly exerts influence on kinetic constant for photodegradation of MB. The  $k$  value for degradation of MB over the  $g\text{-C}_3\text{N}_4$ ,  $\text{NiO}/g\text{-C}_3\text{N}_4$  and  $\text{NiO}/\text{Cd}/g\text{-C}_3\text{N}_4$  (0.05%) nanocomposites are  $20 \times 10^{-4}$ ,  $24 \times 10^{-4}$ , and  $26 \times 10^{-4} \text{ min}^{-1}$ , respectively. By further rising Cd weight percent, the degradation kinetic constant considerably increases and then decreases. The  $k$  value of MB degradation over the  $\text{NiO}/\text{Cd}/g\text{-C}_3\text{N}_4$  (0.1%),  $\text{NiO}/\text{Cd}/g\text{-C}_3\text{N}_4$  (0.2%),  $\text{NiO}/\text{Cd}/g\text{-C}_3\text{N}_4$  (0.4%), and  $\text{NiO}/\text{Cd}/g\text{-C}_3\text{N}_4$  (0.5%) samples are  $141 \times 10^{-4}$ ,  $77 \times 10^{-4}$ ,  $69 \times 10^{-4}$ , and  $62 \times 10^{-4} \text{ min}^{-1}$ , respectively. The nanocomposite with 0.1 wt% Cd exhibits the enhanced kinetic constant for photodegradation of MB, which is 7 and 5.8 times greater than those of the pure  $g\text{-C}_3\text{N}_4$  and  $\text{NiO}/g\text{-C}_3\text{N}_4$  samples, respectively. It is concluded that adding an adequate amount of Cd content might increase the number of active sites, enhance the light absorption capacity, and suppress the recombination of electron-hole pairs. Besides, adding an extra amount of Cd

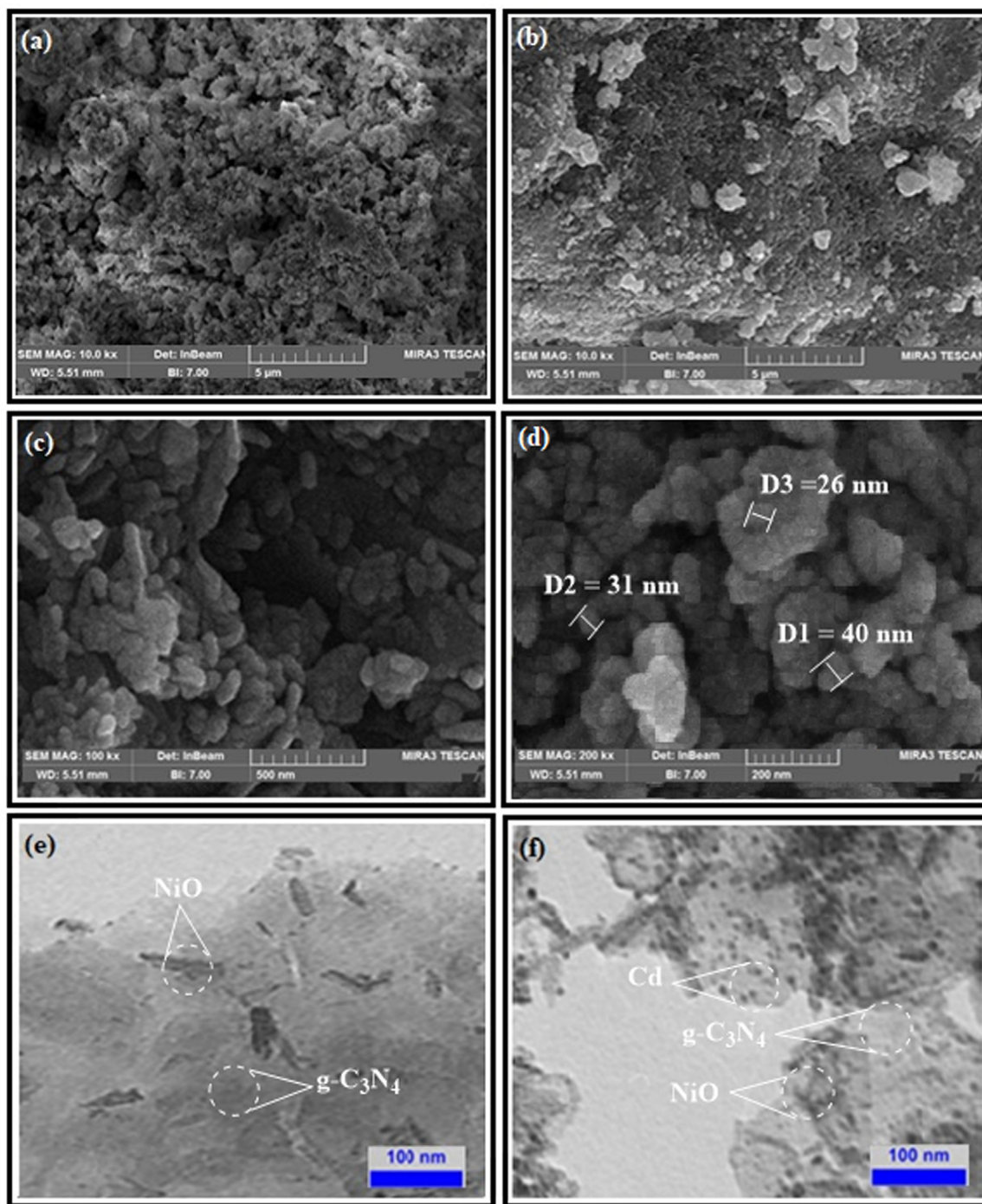


**Fig. 4** The SEM images of the (a) g-C<sub>3</sub>N<sub>4</sub>, (b) NiO/g-C<sub>3</sub>N<sub>4</sub>, (c) and (d) NiO/Cd/g-C<sub>3</sub>N<sub>4</sub> (0.1%) nanocomposites. The TEM images of the (e) NiO/g-C<sub>3</sub>N<sub>4</sub>, and (f) NiO/Cd/g-C<sub>3</sub>N<sub>4</sub> (0.1%) nanocomposites.

species might fill and block some of the active sites on the surface of the nanocomposites, resulting in the reduction of photocatalytic activity.

### 3.3. Photocatalytic mechanism

The reasonable mechanism for degradation of MB over the NiO/Cd/g-C<sub>3</sub>N<sub>4</sub> (0.1%) nanocomposite under the visible light irradiation is depicted in Fig. 8a. Photons with energy equal to

or greater than the bandgaps of the semiconductor counterparts of the nanocomposite generate electron-hole pairs (Yang et al., 2016). As the photogenerated electrons transit from the valence band (VB) to the conduction band (CB), leave behind them empty spaces called the holes (Chang et al., 2014). Free electrons and holes make a negative mass on CB and a positive mass on VB, respectively, and take part in the chemical redox reactions at the surface of the nanocomposite (Han et al., 2015).

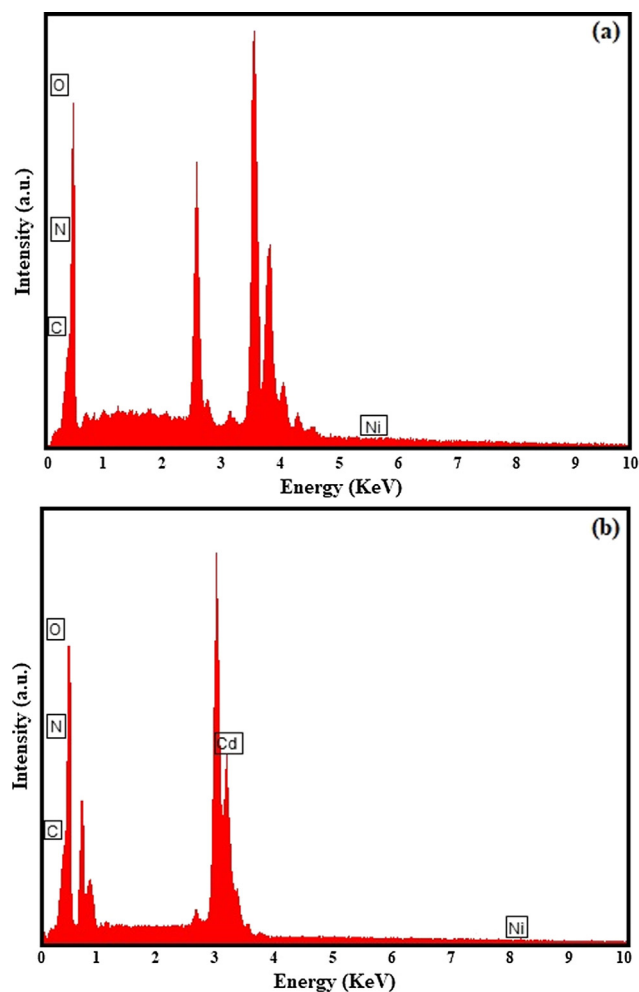


**Fig. 5** The EDS spectra of the (a) NiO/g-C<sub>3</sub>N<sub>4</sub> and (b) NiO/Cd/g-C<sub>3</sub>N<sub>4</sub> (0.1%) nanocomposites.

Concerning Butler and Ginley model, electron transfer mode depends on CB and VB energies of the semiconductors at the point of zero charges, calculated by the following equations:

$$E_{CB} = X - E^c - 0.5E_g \quad (3)$$

$$E_{VB} = X - E^c + 0.5E_g \quad (4)$$

where X is the absolute electronegativity of the semiconductor,  $E^c$  is the energy of free electrons on the hydrogen scale (4.5 eV), and  $E_g$  is the bandgap energy of the semiconductor (Mousavi and Habibi-Yangjeh, 2015).

The CB and VB energies of g-C<sub>3</sub>N<sub>4</sub> and NiO were calculated -1.12, 1.58 eV, and -3.15, 0.45 eV, respectively. Under the visible light irradiation, electrons from the VB transit to the CB of g-C<sub>3</sub>N<sub>4</sub> and NiO counterparts of the NiO/Cd/g-C<sub>3</sub>N<sub>4</sub> nanocomposite, owing to their low  $E_g$  values, 2.7 and 3.6 eV, respectively. As illustrated in Fig. 8a, the numerical value of the CB and VB energies of g-C<sub>3</sub>N<sub>4</sub> are greater than those of NiO, so the transfer mode of electrons and holes may be consistent with the Z-scheme-based system (ZBS), a broader redox mechanism which represents more positive VB and more negative CB potentials (Mishra et al., 2019;

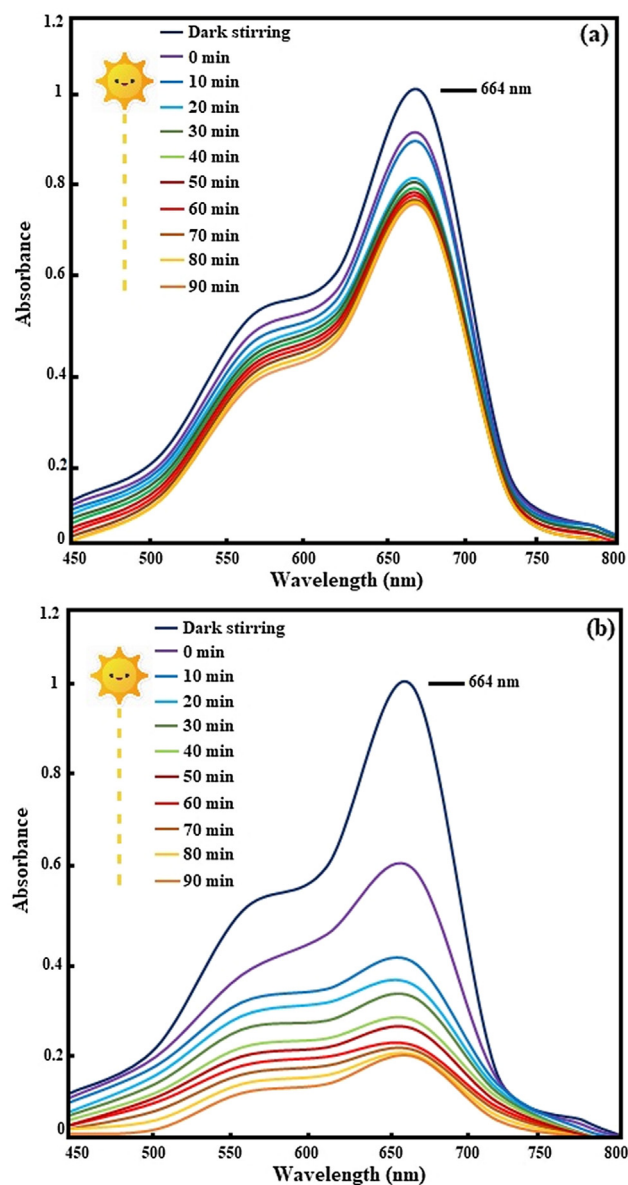


**Fig. 6** The UV/Vis spectra for degradation of MB under the visible light irradiation over the (a) NiO/g-C<sub>3</sub>N<sub>4</sub> and (b) NiO/Cd/g-C<sub>3</sub>N<sub>4</sub> (0.1%) nanocomposites.

Patnaik et al., 2018; Acharya et al., 2017). Due to the more negative potential of the CB of NiO compared with that of g-C<sub>3</sub>N<sub>4</sub>, some of the photogenerated electrons easily transfer from the CB of NiO to the CB of g-C<sub>3</sub>N<sub>4</sub>. Furthermore, a number of the electrons react with the adsorbed O<sub>2</sub> molecules to produce  $\cdot O_2^-$ , because the potential of O<sub>2</sub>/O<sub>2</sub><sup>-</sup> (-0.33 eV) is more positive than the potentials of the CB of the semiconductors (Tian et al., 2019). On the other hand, the potential of O<sub>2</sub>/H<sub>2</sub>O<sub>2</sub> (0.69 eV) is more positive than the CB potentials of g-C<sub>3</sub>N<sub>4</sub> and NiO. Hence, the electrons on the CB can reduce O<sub>2</sub> to H<sub>2</sub>O<sub>2</sub> and form  $\cdot OH$  radicals by capturing electrons (Jiang et al., 2012). Besides, some of the accumulated electrons on the CB of g-C<sub>3</sub>N<sub>4</sub> transfer to cadmium-rich sites. Cd ions effectively promote the separation of electron-hole pairs, prolonging the lifetime of photoinduced charge carriers and enhance

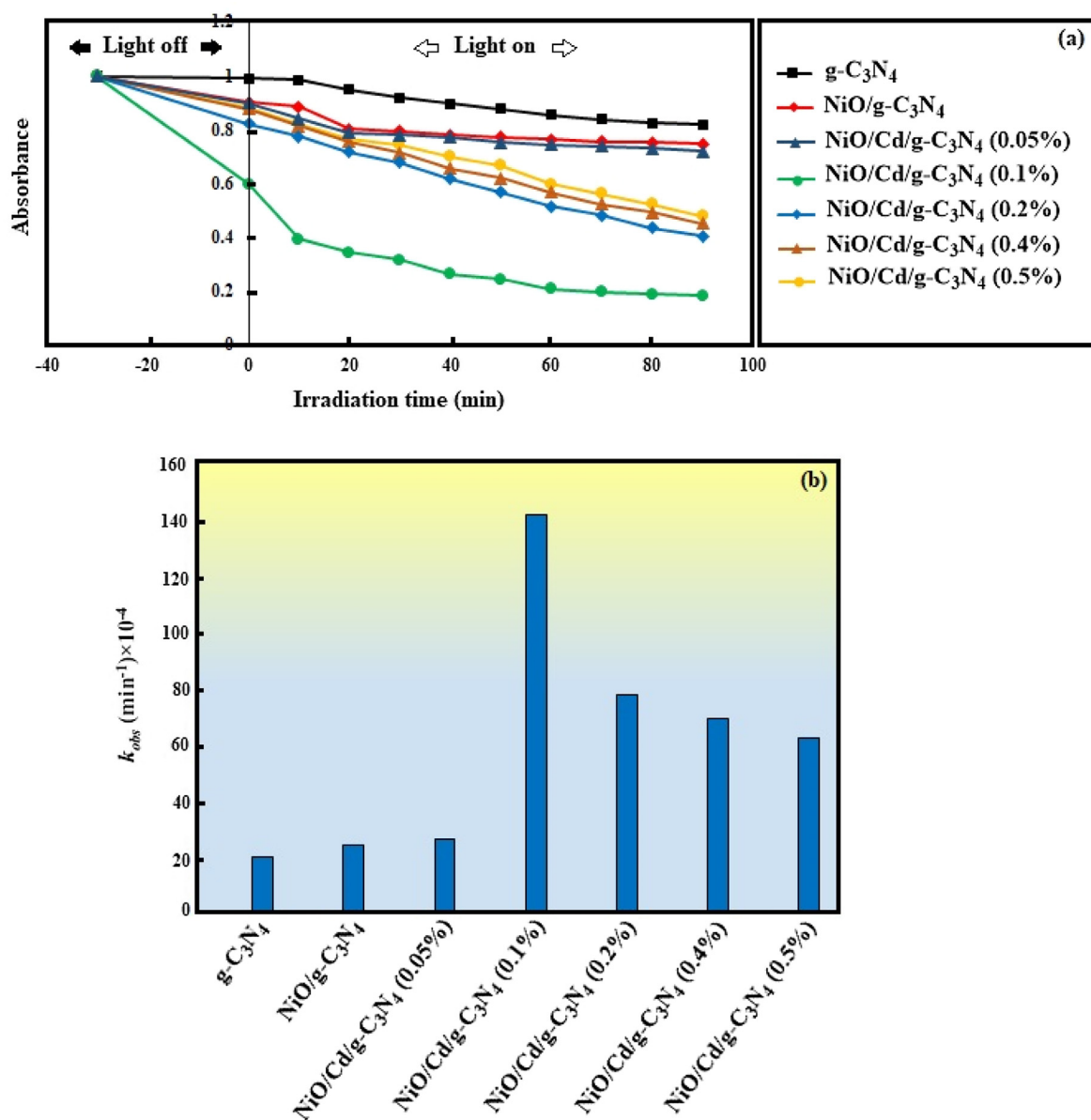


**Fig. 7** (a) The photocatalytic degradation of MB over the g-C<sub>3</sub>N<sub>4</sub>, NiO/g-C<sub>3</sub>N<sub>4</sub>, and NiO/Cd/g-C<sub>3</sub>N<sub>4</sub> nanocomposites with different weight percent of Cd. (b) The kinetic constant of MB degradation reaction over the different nanocomposites.

the photocatalytic efficiency. From the thermodynamic point of view, the electrons and holes immigrate in the opposition direction. The VB potential of g-C<sub>3</sub>N<sub>4</sub> is more positive than that of NiO. As a consequence, the photogenerated holes transfer from the VB of g-C<sub>3</sub>N<sub>4</sub> to the VB of NiO. Since the potentials of ·OH/H<sub>2</sub>O (2.72 eV) and ·OH/<sup>-</sup>OH (2.38 eV) is higher than the VB potentials of the semiconductors, the photogenerated holes cannot react with the adsorbed H<sub>2</sub>O and <sup>-</sup>OH to produce ·OH radicals (He et al., 2013). The superoxide radical anion ·O<sub>2</sub><sup>-</sup>, hydroxyl radical ·OH, and the holes are known as the reactive species that decompose methylene blue molecules to CO<sub>2</sub>, H<sub>2</sub>O, and final degradation products (inorganic salts) without any secondary pollutants.

A series of scavengers were added to the system to reveal the major reactive species in the degradation of MB. Fig. 8b shows the plot of the degradation kinetic constant ( $k$ ) in the presence of BQ (scavenger of ·O<sub>2</sub><sup>-</sup>), 2-PrOH (scavenger of ·OH), and KI (scavenger of the holes) (Mousavi and Habibi-Yangjeh, 2015). As can be seen, the  $k$  value without using any scavenger decreased from  $141 \times 10^{-4}$  to  $12 \times 10^{-4}$ ,  $32 \times 10^{-4}$ , and  $38 \times 10^{-4} \text{ min}^{-1}$  in the presence of BQ, 2-PrOH, and KI, respectively. The decrease of  $k$  value in the presence of BQ is much higher than those of 2-PrOH and KI scavengers. As a result, ·O<sub>2</sub><sup>-</sup> plays a significant role in the degradation of MB over the NiO/Cd/g-C<sub>3</sub>N<sub>4</sub> (0.1%) nanocomposite.



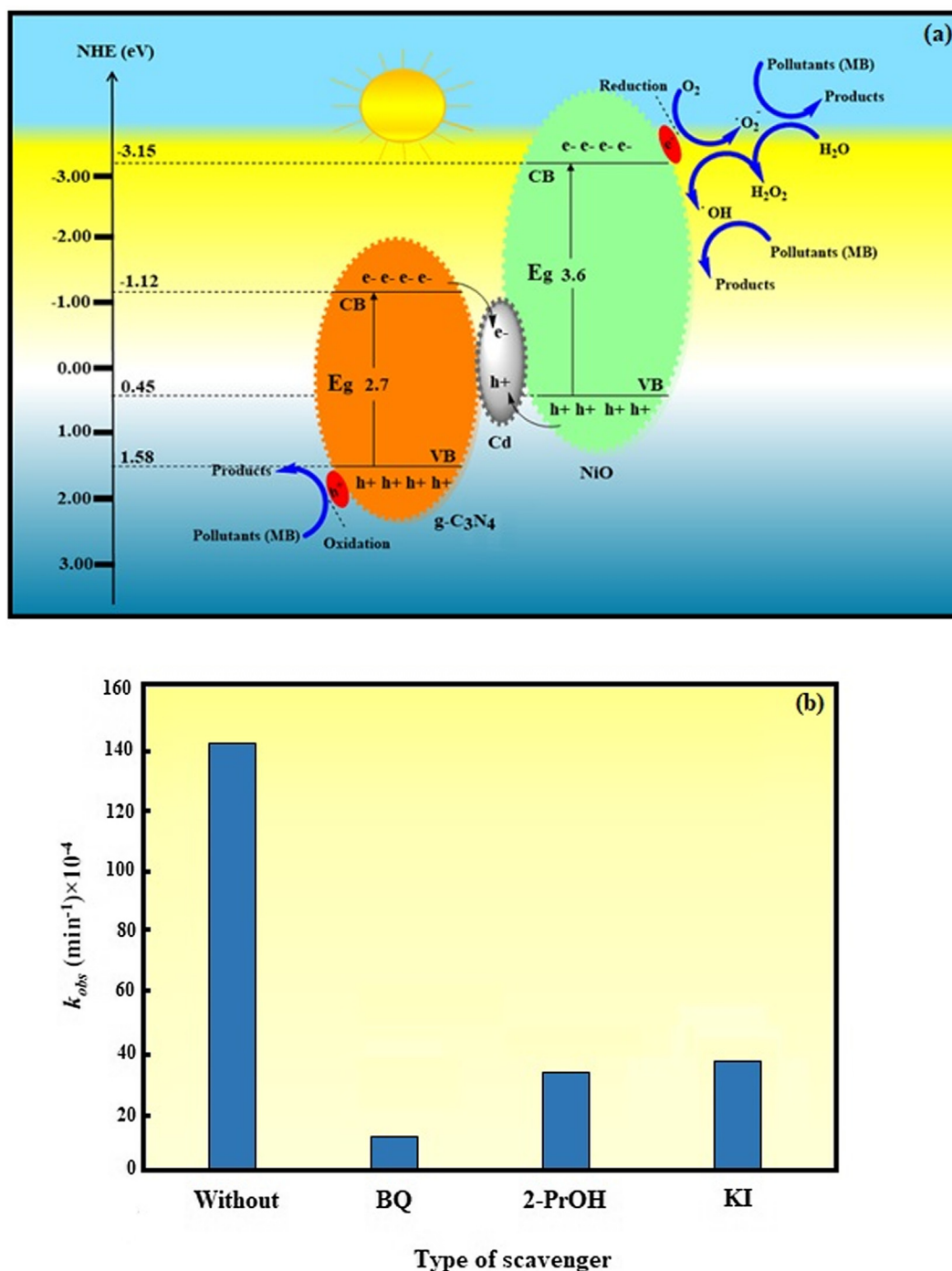


**Fig. 8** (a) The schematic illustration for the possible mechanism of MB degradation over the NiO/Cd/g-C<sub>3</sub>N<sub>4</sub> (0.1%) nanocomposite. (b) The degradation kinetic constant of MB over the NiO/Cd/g-C<sub>3</sub>N<sub>4</sub> (0.1%) nanocomposite in the presence of different scavengers.

### 3.4. Reusability test

From the viewpoint of economic efficiency, stability and lifetime of photocatalysts are essential factors. In this study, the photodegradation experiments were carried out four times under the same conditions to show the reusability of the NiO/Cd/g-C<sub>3</sub>N<sub>4</sub> (0.1%) nanocomposite. In each recycling run, the catalyst was collected by centrifugation, washed

with ethanol/DI water, and calcined at 550 °C for two hours. As shown in Fig. 9, after four repeated runs, no remarkable decrease in the photocatalytic activity occurred. MB molecules were successfully degraded at the rate of 81.8, 81.5, 80.6, and 80.1% in the 1st, 2nd, 3rd, and 4th runs, respectively. It means that the NiO/Cd/g-C<sub>3</sub>N<sub>4</sub> (0.1%) nanocomposite has a useful life and can be suitable for practical applications.

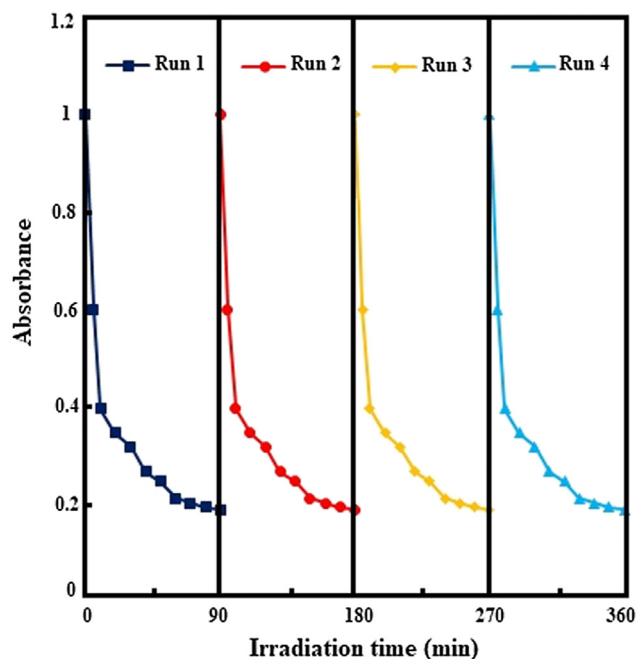


**Fig. 9** Reusability of the NiO/Cd/g-C<sub>3</sub>N<sub>4</sub> (0.1%) nanocomposite for four successive runs.

#### 4. Conclusions

Briefly, we successfully prepared a series of novel NiO/Cd/g-C<sub>3</sub>N<sub>4</sub> nanocomposites with different weight percent of cadmium using the green and straightforward microwave-assisted method. The as-synthesized nanocomposites were characterized by XRD, FT-IR, BET, SEM, TEM, EDS, and UV-Vis analytical techniques. Photocatalytic activity of the visible-light-driven photocatalysts was evaluated by the degradation of MB aqueous solution at room temperature. The results demonstrated that the weight percent of cadmium had a remarkable influence on the degradation reaction. The enhanced photocatalytic activity of the nanocomposite with 0.1 wt% Cd was attributed to the Z-scheme charge transfer mode, resulting in a more effective separation of photogenerated electron-hole pairs. Then ·O<sub>2</sub> radicals were recognized as the main active species during the reaction by the radical trapping experiments. Finally, the reusability of the nanocomposite was confirmed after four consecutive runs.

#### Declaration of Competing Interest

The authors declare that they have no known competing financial interests or personal relationships that could have appeared to influence the work reported in this paper.

#### Acknowledgment

The Iran National Science Foundation (INSF), Iran and Payame Noor University are gratefully acknowledged for financial support of this work (Grant No. 95006259), Iran.

#### References

- Acharya, S., Mansingh, S., Parida, K.M., 2017. *Inorg. Chem. Front.* 4 (6), 1022–1032.
- Akhundi, A., Habibi-Yangjeh, A., 2015. *Ceram. Int.* 41, 5634–5643.
- Akhundi, A., Habibi-Yangjeh, A., 2017. *J. Colloid Interface Sci.* 504, 697–710.
- Allahresani, A., Nasser, M.A., Nakhaei, A., 2017. *Res. Chem. Intermed.* 43, 6367–6378.
- Allahresani, A., Taheri, B., Nasser, M.A., 2018. *Res. Chem. Intermed.* 44, 1173–1188.
- Babu, P., Mohanty, S., Naik, B., Parida, K., 2018. *ACS Appl. Energy Mater.* 1 (11), 5936–5947.
- Babu, P., Mohanty, S., Naik, B., Parida, K.M., 2019. *Inorg. Chem.* 58 (18), 12480–12491.
- Bian, Z., Tachikawa, T., Cui, S.C., Fujitsuka, M., Majima, T., 2012. *Chem. Sci.* 3, 370–379.
- Chang, C., Zhu, L., Wang, S., Chu, X., Yue, L., 2014. *ACS Appl. Mater. Interfaces.* 6, 5083–5093.
- Cui, Y., Zhang, G., Lin, Z., Wang, X., 2016. *Appl. Catal. B.* 181, 413–419.
- Das, K.K., Patnaik, S., Mansingh, S., Behera, A., Mohanty, A., Acharya, C., Parida, K.M., 2020. *J. Colloid Interf. Sci.* 561, 551–567.
- Deng, Y., Tang, L., Feng, C., Zeng, G., Wang, J., 2018. *J. Hazard. Mater.* 344, 758–769.
- Dharmaraj, N., Prabhu, P., Nagarajan, S., Kim, C.H., Park, J.H., Kim, H.Y., 2006. *Mater. Sci. Eng. B.* 128, 111–114.
- Green, M., Liu, Z., Smedley, R., Nawaz, H., Li, X., Huang, F., Chen, X., 2018. *Mater. Today Phys.* 5, 78–86.
- Habibi, M.H., Rahmati, M.H., 2014. *Spectrochim. Acta. A.* 133, 13–18.
- Han, H., Fu, M., Li, Y., Guan, W., Lu, P., Hu, X., 2018. *Chin. J. Catal.* 39, 831–840.
- Han, C., Wang, Y., Lei, Y., Wang, B., Wu, N., Shi, Q., Li, Q., 2015. *Nano Res.* 8, 1199–1209.
- He, Z., Shi, Y., Gao, C., Wen, L., Chen, J., Song, S., 2013. *J. Phys. Chem. C.* 118, 389–398.
- Huang, H., Xiao, K., Tian, N., Dong, F., Zhang, T., Du, X., Zhang, Y., 2017. *J. Mater. Chem. A.* 5, 17452–17463.
- Jeejamol, D.J., Raj, A.M.E., Jayakumari, K., Ravidhas, C., 2018. *J. Mater. Sci. Mater. Electron.* 29, 97–116.
- Jiang, J., Li, H., Zhang, L., 2012. *Chem. Eur. J.* 18, 6360–6369.
- Karimi, M.A., Hatefi-Mehrjardi, A., Kabir, A.A., Zaydabadi, M., 2015. *Res. Chem. Intermed.* 41, 6157–6168.
- Kumar, V., Rajaram, P., Goswami, Y.C., 2017. *J. Mater. Sci. Mater. Electron.* 28, 9024–9031.
- Kumaresan, N., Sinthiya, M.M.A., Kumar, M.P., Ravichandran, S., Babu, R.R., Sethurman, K., Ramamurthi, K., 2020. *Arab. J. Chem.* 13, 2826–2843.
- Lai, S.H., Chen, Y.B., Li, N., Su, H., Guo, S.H., 2018. *J. Mater. Sci. Mater. Electron.* 29, 4509–4516.
- Li, M., Liao, H., Deng, Q., Wu, Y., Xiao, F., Wei, X., Tu, D., 2018. *J. Macromol. Sci. A.* 55, 408–413.
- Li, F.T., Zhao, Y., Wang, Q., Wang, X.J., Hao, Y.J., Liu, R.H., Zhao, D., 2015. *J. Hazard. Mater.* 283, 371–381.
- Lu, M., Pei, Z., Weng, S., Feng, W., Fang, Z., Zheng, Z., Liu, P., 2014. *Phys. Chem. Chem. Phys.* 16, 21280–21288.
- Lu, X., Xie, J., Jeffery, A.A., Chen, X., Li, X., 2019. *Appl. Catal. B.* 252, 250–259.
- Lu, Z., Zeng, L., Song, W., Qin, Z., Zeng, D., Xie, C., 2017. *Appl. Catal. B.* 202, 489–499.
- Martha, S., Nashim, A., Parida, K.M., 2013. *J. Mater. Chem. A* 1. 26, 7816–7824.
- Mella, B., Barcellos, B.S.D.C., Da Silva Costa, D.E., Gutterres, M., 2017. *Ozone Sci. Eng.* 40, 133–140.

- Mishra, P., Behera, A., Kandi, D., Parida, K., 2019. *Nanoscale Adv.* 1, 5, 1864–1879.
- Mousavi, M., Habibi-Yangjeh, A., 2015. *Mater. Chem. Phys.* 163, 421–430.
- Mousavi, M., Habibi-Yangjeh, A., Pourn, S.R., 2018. *J. Mater. Sci. Mater. Electron.* 29, 1719–1747.
- Mousavi, M., Habibi-Yangjeh, A., 2018. *J. Mater. Sci.* 53, 9046–9063.
- Nagajyothi, P.C., Pandurangan, M., Vattikuti, S.V.P., Tettey, C.O., Sreekanth, T.V.M., Shim, J., 2017. *Sep. Purif. Technol.* 188, 228–237.
- Nayak, S., Parida, K.M., 2018. *ACS Omega* 3 (7), 7324–7343.
- Nayak, S., Parida, K.M., 2019. *Sci. Rep.* 9 (1), 1–23.
- Nezar, S., Cherifi, Y., Barras, A., Addad, A., Dogheche, E., Saoula, N., Laoufi, N., Roussel, P., Szunerits, S., Boukherroub, R., 2018. *Arab. J. Chem.* 01, 1–10.
- Patnaik, S., Das, K.K., Mohanty, A., Parida, K., 2018. *Catal. Today* 315, 52–66.
- Patnaik, S., Sahoo, D.P., Parida, K., 2018. *Renew. Sust. Energ. Rev.* 82, 1297–1312.
- Patnaik, S., Swain, G., Parida, K.M., 2018. *Nanoscale* 10, 13, 5950–5964.
- Peng, D., Wang, H., Yu, K., Chang, Y., Ma, X., Dong, S., 2016. *RSC Adv.* 6, 77760–77767.
- Pirhashemi, M., Habibi-Yangjeh, A., 2013. *Appl. Surf. Sci.* 283, 1080–1088.
- Su, F.Y., Xu, C.Q., Yu, Y.X., Zhang, W.D., 2016. *Chem. Cat. Chem.* 8, 3527–3535.
- Tian, N., Huang, H., Du, X., Dong, F., Zhang, Y., 2019. *J. Mater. Chem. A* 7, 11584–11612.
- Wang, K., Li, Q., Liu, B., Cheng, B., Ho, W., Yu, J., 2015. *Appl. Catal. B.* 176, 44–52.
- Wang, D., Li, J., Xu, Z., Zhu, Y., Chen, G., Cui, Z., 2019. *J. Mater. Sci.* 54, 11417–11434.
- Wang, Q., Zheng, L., Chen, Y., Fan, J., Huang, H., Su, B., 2015. *J. Alloy. Compd.* 637, 127–132.
- Wen, J., Xie, J., Zhang, H., Zhang, A., Liu, Y., Chen, X., Li, X., 2017. *ACS Appl. Mater. Interfaces.* 9, 14031–14042.
- Wen, J., Xie, J., Yang, Z., Shen, R., Li, H., Luo, X., Chen, X., Li, X., 2017. *ACS Sust. Chem. Eng.* 5, 2224–2236.
- Wu, Y., Wang, Y., Di, A., Yang, X., Chen, G., 2018. *Catal. Lett.* 148, 2179–2189.
- Xu, Y., Huang, S., Xie, M., Li, Y., Xu, H., Huang, L., Li, H., 2015. *RSC Adv.* 5, 95727–95735.
- Yan, S.C., Li, Z.S., Zou, Z.G., 2009. *Langmuir.* 25, 10397–10401.
- Yang, C.T., Lee, W.W., Lin, H.P., Dai, Y.M., Chi, H.T., Chen, C.C., 2016. *RSC Adv.* 6, 40664–40675.
- Yin, S., Han, J., Zhou, T., Xu, R., 2015. *Catal. Sci. Technol.* 5, 5048–5061.
- Zhang, L., Huang, F., Liang, C., Zhou, L., Zhang, X., Pang, Q., 2016. *J. Taiwan Inst. Chem. E.* 60, 643–650.
- Zhou, M., Hou, Z., Zhang, L., Liu, Y., Gao, Q., Chen, X., 2017. *Sust. Energy Fuels.* 1, 317–323.
- Zhou, M., Hou, Z., Chen, X., 2018. *Part. Part. Syst. Char.* 35, 1700038–1700046.